Direct Measurement of Anharmonic Decay Channels of a Coherent Phonon

Samuel W. Teitelbaum,[1,2] Tom Henighan,[1,3] Yijing Huang,[1,4] Hanzhe Liu,[1,3] Mason P. Jiang,[3,1] Diling Zhu,[5] Matthieu Chollet,[5] Takahiro Sato,[5] Éamonn D. Murray,[6] Stephen Fahy,[7,8] Shane O'Mahony,[7,8] Trevor P. Bailey,[9] Ctirad Uher,[9] Mariano Trigo,[1,2] and David A. Reis[1,2,4,10]

[1] *PULSE Institute of Ultrafast Energy Science, SLAC National Accelerator Laboratory, Menlo Park, California 94025, USA*
[2] *Stanford Institute for Materials and Energy Sciences, SLAC National Accelerator Laboratory, Menlo Park, California 94025, USA**
[3] *Department of Physics, Stanford University, Stanford, California 94305, USA*
[4] *Department of Applied Physics, Stanford University, Stanford, California 94305, USA*
[5] *LCLS, SLAC National Accelerator Laboratory, Menlo Park, California 94025, USA*
[6] *Department of Physics and Department of Materials, Imperial College London, London SW7 2AZ, United Kingdom*
[7] *Tyndall National Institute, Cork, Ireland*
[8] *Department of Physics, University College Cork, Cork, Ireland*
[9] *Department of Physics, University of Michigan, Ann Arbor, Michigan 48109, USA*
[10] *Department of Photon Science, Stanford University, Stanford, California 94305, USA*

(Dated: August 28, 2018)

We report channel-resolved measurements of the anharmonic coupling of the coherent A_{1g} phonon in photoexcited bismuth to pairs of high wavevector acoustic phonons. The decay of a coherent phonon can be understood as a parametric resonance process whereby the atomic displacement periodically modulates the frequency of a broad continuum of modes. This coupling drives temporal oscillations in the phonon mean-square displacements at the A_{1g} frequency that are observed across the Brillouin zone by femtosecond x-ray diffuse scattering. We extract anharmonic coupling constants between the A_{1g} and several representative decay channels that are within an order of magnitude of density functional perturbation theory calculations.

Lattice anharmonicity governs a broad range of phenomena in condensed matter physics, from structural phase transitions [1] to heat transport and thermoelectricity [2, 3]. Recent advances in first-principles calculations have allowed for precise calculations of thermal properties including effects due to phonon-phonon scattering [4–7]. However, experimental probes of the microscopic details of anharmonicity remain elusive. While scattering techniques like inelastic neutron scattering [8–10] and inelastic x-ray scattering [11–14] can measure properties of phonons such as frequencies and lifetimes across the Brillouin zone, these techniques lack the ability to resolve the individual decay channels of a given mode. Such a measurement would provide a unique view of the phonon-phonon scattering processes occurring during thermal equilibration, including a quantitative measurement of anharmonic force constants.

We report direct measurements of the anharmonic coupling of the zone center Raman active A_{1g} optic phonon in bismuth to longitudinal acoustic phonons at high wavevector, and extract anharmonic coupling constants for a subset of these modes that are within an order of magnitude of that obtained by a first-principles based model. These measurements utilize femtosecond x-ray diffuse scattering to probe the temporal evolution of the phonon mean square displacements following optical excitation [15]. It was proposed in [16] that a parametric resonance of the zone-center mode with the acoustic branch would be observable in femtosecond scattering measurements using an x-ray free electron laser (FEL).

Bismuth is a group V semimetal that exhibits particularly strong electron-phonon coupling due to its Peierls distorted structure, making it an ideal testbed for the study of large-amplitude phonon motion. Upon photoexcitation, the sudden change in the lattice potential causes the atoms to move coherently along the A_{1g} mode coordinate, resulting in a macroscopic modulation of both the optical reflectivity [17–19] and the Bragg peaks that are sensitive to the A_{1g} structure factor modulation [20–22].

We use the self-consistent theoretical framework developed in reference [16] to describe the anharmonic coupling of the photoexcited coherent phonon to pairs of phonons with large wavevector (target modes), in a process analogous to optical parametric downconversion (as shown schematically in Fig. 1(a)). The Hamiltonian describing cubic coupling of a single mode with normal mode amplitude and momentum (U_0, P_0) to a branch of N modes with reduced wavevector $\boldsymbol{q}$ can be expressed as

$$H = \frac{1}{2}\left[P_0^2 + \Omega^2 U_0^2\right] + \frac{1}{2N}\sum_{\boldsymbol{q}}\left[p_{\boldsymbol{q}}^2 + \omega_{\boldsymbol{q}}^2(1 + 2g_{\boldsymbol{q}}U_0)u_{\boldsymbol{q}}^2\right], \tag{1}$$

where $p_{\boldsymbol{q}}$ and $u_{\boldsymbol{q}}$ are the corresponding normal mode momentum and displacement and $g_{\boldsymbol{q}}$ specifies the strength of the anharmonic coupling between the zone-center phonon and phonons at $\pm\boldsymbol{q}$ [16]. Note that a coherent zone-center phonon has $\langle U_0\rangle \sim 1-\cos(\Omega t)$ such that it parametrically modulates the frequency of the other phonons, driving squeezing oscillations in their mean square displacements

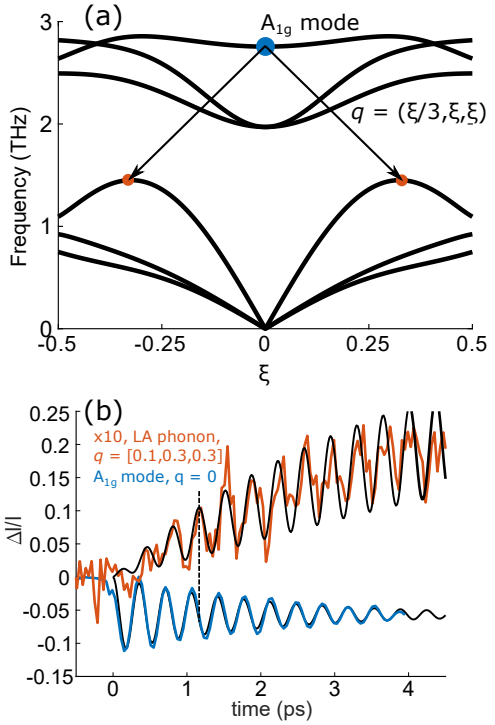

Figure 1. Color online. (a) Phonon dispersion relation in bismuth along the $\boldsymbol{q} = (\frac{1}{3}\xi\ \xi\ \xi)$ direction, illustrating a decay channel of an A_{1g} phonon into a pair of LA phonons at $\boldsymbol{q}$ and $-\boldsymbol{q}$. (b) experimental signature of decay of the A_{1g} phonon in bismuth by the channel shown in (a). The lower (blue) curve shows the relative intensity change of the (2 3 2) Bragg peak, which is proportional to the A_{1g} mode amplitude. The upper (orange) curve shows the relative intensity change of the diffuse scattering $\Delta I/I$ in a region near $\boldsymbol{q} = (0.1\ 0.3\ 0.3)$ in the (0 1 1) zone (multiplied by 10). The black lines are simulations. The dashed line indicates a $\pi/2$ phase shift between the A_{1g} mode and the target mode.

[16, 23, 24]

$$\Delta\left\langle u_q^2(t)\right\rangle = \frac{\mp kTg_qA}{\omega_q\sqrt{(\gamma')^2+(2\omega_q-\Omega)^2}}\left[e^{-\gamma_0 t/2}\sin(\Omega t+\delta') - e^{-\gamma_q t}\sin(2\omega_q t+\delta')\right], \quad (2)$$

where A and γ_0 are the amplitude and (energy) damping rate of the coherently excited driving mode at frequency Ω. $\omega_{\boldsymbol{q}}$ and $\gamma_{\boldsymbol{q}}$ are the frequency and damping rate of the target mode at q. $\gamma' = \gamma_q - \gamma_0/2$ and $\delta' = \tan^{-1}[(2\omega_{\boldsymbol{q}} - \Omega)/(\gamma_{\boldsymbol{q}} - \gamma_0/2)]$. The negative (positive) sign corresponds to $\gamma' > 0$ ($\gamma' < 0$), and the "Δ" means that we have subtracted off the thermal equilibrium value before excitation. Note the squeezing is most effective when the parametric resonance condition is met, *i.e.* $\Omega = 2\omega_{\boldsymbol{q}}$. [25]. In Eq. 2, we have taken the target mode occupation to be classical, which is appropriate for bismuth at room temperature.

The experiment was carried out using the XPP instrument at the LCLS x-ray FEL with a photon energy of 9.5 keV from a diamond double-crystal monochromator[26]. The sample was rotated such that the x rays propagated at a 71 deg. angle with respect to $(2\bar{1}\bar{1})$ (binary axis). 800 nm, $\sim$ 45 fs pump pulses were focused onto a 50 nm thick (111) epitaxial Bi film on BaF_2 at a 1.8 degree angle of incidence with respect to the surface with an incident fluence of 2.5 mJ/cm^2. The x-ray pulses were less than 50 fs in duration and contained $\sim 10^9$ photons per shot at a repetition rate of 120 Hz. The x rays were incident on the sample at an angle of 0.5 degrees relative to the surface so that their penetration depth matched the thickness of the Bi film. The delay between the optical and x-ray pulses was controlled using a fast-scan delay stage, and the fine timing was measured on a single-shot basis using the XPP timing tool [26]. The overall time resolution of the instrument is better than 100 fs, allowing observation of oscillations in the x-ray intensity to $\sim$5 THz, more than sufficient to measure the coherent A_{1g} mode at 2.82 THz. A polycrystalline LaB_6 sample was used for calibration of the pixel array detector (CSPAD [27]) position used to simultaneously collect scattered x rays over a wide range of momentum transfer $\boldsymbol{Q}$.

Fig. 1(a) shows the calculated phonon dispersion of Bi along the $\boldsymbol{q} = (\xi/3\ \xi\ \xi)$ direction. The arrows show one particular decay channel of the A_{1g} mode, corresponding to the data shown in Fig. 1(b). The lower curve shows the relative intensity change $\Delta I/I$ near the (2 3 2) Bragg peak, which oscillates in time with the coherent A_{1g} mode displacement. The oscillations are fit to a decaying cosine function, which is used to extract the amplitude of the A_{1g} mode from the structure factor. The upper plot is the relative intensity change (multiplied by 10) in the diffuse scattering around $\boldsymbol{q} = (0.1\ 0.3\ 0.3)$ reciprocal lattice units (r.l.u.), where the (highest) acoustic phonon frequency $\omega_{\boldsymbol{q}}$ is close to half of Ω_{A1g}. The intensity oscillations in this region are attributed to resonantly squeezed phonons with predominantly LA character driven by anharmonic coupling with the A_{1g} mode, described in more detail below. The black curves show simulation results for the diffuse scattering in a region around $\boldsymbol{Q} = (0.1\ 1.3\ 1.3)$ r.l.u., derived from Eq. (2), which also includes a slow increase of the diffuse scattering to account for the slow heating of the lattice due to incoherent electron-phonon coupling [28–30], and a fit to the Bragg peak time dependence due to modulation of the A_{1g} mode displacement. From the A_{1g} mode oscillation, we extract a softened frequency of 2.82 THz, and an amplitude of $A = 9.74\times10^{-4}$ (in units of the c-axis of bismuth), or 1.15 pm, and a decay rate of $\gamma_0 = 0.82$ ps^{-1}. The extracted amplitude is in good agreement with previous measurements with similar bond softening [21].

We extract $u_q^2(t)$ from the time-dependent diffuse scattering intensity. For a particular mode on branch i, the partial contribution to the scattered intensity at scatter-

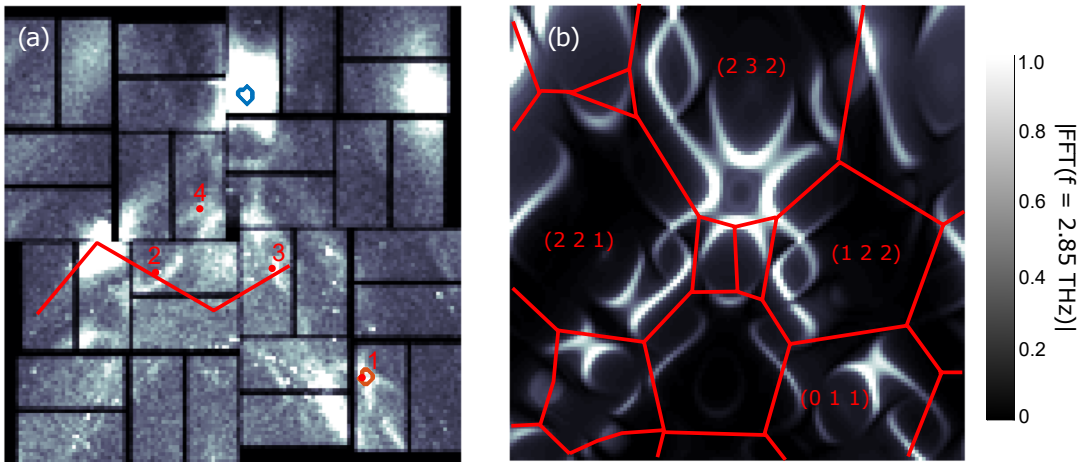

Figure 2. Color online. (a) Intensity map of the Fourier transform of the femtosecond diffuse scattering signal at $f = 2.85$ THz. The red line is the path of the lineout shown in Fig. 3. The points labeled (1)-(4) are used to extract the coupling constants shown in table I. The blue and orange boxes outline the regions used to extract the time-domain traces in Fig. 1. The four brightest spots in (a) are due to oscillations of the structure factor from the A_{1g} mode near Bragg peaks and are therefore not present in (b). Brillouin zones relevant to the text are labeled in (b). (b) Predicted intensity map using the dispersion relation of bismuth and the parametric resonance condition, with a uniform anharmonic coupling constant $g = 1.0$. The red lines in (b) show the Brillouin zone boundaries.

ing vector $\boldsymbol{Q}$ is

$$I_i(\boldsymbol{Q}) \propto \langle u^2_{\boldsymbol{q},i} \rangle \left| \sum_s \boldsymbol{Q} \cdot \boldsymbol{\epsilon}^{(s)}_{\boldsymbol{q},i} e^{i\boldsymbol{Q}\cdot\boldsymbol{r}_s} \right|^2 \qquad (3)$$

Here $\boldsymbol{r}_s$ is the equilibrium position and $\boldsymbol{\epsilon}^{(s)}_{\boldsymbol{q},i}$ is the eigenvector corresponding to the sth atom in the unit cell. The frequencies and eigenvectors are taken from density functional perturbation theory calculations.

From the measured amplitudes, we extract anharmonic coupling constants $g_{\boldsymbol{q}}$ from (2). The only adjustable parameter is the target mode decay $\gamma_{\boldsymbol{q}}$, which we estimate to be 0.3 ps^{-1} from the measured decay rate of non-resonant two-phonon coherences in the frequency range of 1–2 THz.[31].

Thus, we extract an anharmonic coupling constant of $g_{\boldsymbol{q}} = -1.0$ for $\boldsymbol{q} = (0.1\ 0.3\ 0.3)$ r.l.u. An amplitude of 1.0 means that for a 1% displacement in the position of the bismuth atom along the A_{1g} mode (relative to the c-axis) there is a 1% change in the LA phonon frequency. Here we have chosen a convention whereby the negative sign means that as the atom moves toward the center of the unit cell (U_0 negative), the LA phonon mode hardens.

The uncertainty in the measured values of the coupling constants are primarily due to systematic errors. These errors are associated with our estimate of the decay rate of the target mode $\gamma_{\boldsymbol{q}}$, and our extraction of the scattered intensity from the squeezed mode, $I_i(\boldsymbol{Q})$, from $\Delta I/I$. We estimate $\gamma_{\boldsymbol{q},i} =$ 0.3 ps^{-1} based on the damping rate for acoustic modes near 1 THz (generated by sudden squeezing due to photoexcitation). The measured value of $\langle u^2_{\boldsymbol{q},i} \rangle$ depends on the ability to separate the contribution from a single mode from other sources of scattering at $\boldsymbol{Q}$, including diffuse scattering from other phonons as well as other sources (*e.g.* due to static disorder and Compton scattering).

DFT frozen-phonon calculations predict a value of $g_{\boldsymbol{q}} = -8.4$ for the decay channel shown in fig 1, which is within an order of magnitude of our experimentally measured value. When summing over the Brillouin zone, the calculations predict an A_{1g} phonon decay rate of 0.34 ps^{-1} [16] at room temperature, in reasonable agreement with the experimentally determined decay rate at low fluence of 0.5 ps^{-1} [32], and 0.82 ps^{-1} for the excitation conditions used in this work.

For a fixed experimental geometry, we are able to observe the anharmonic decay to modes covering a large portion of the Brillouin zone. In order to identify these modes, we look for regions of diffuse scattering that show intensity oscillations at f_{A1g}(2.85 THz). This is accomplished by taking a Fourier transform along the time axis for each detector pixel, and plotting the intensity of the Fourier transform at the frequency frame closest to the A_{1g} mode frequency. The resulting intensity map is shown in Fig. 2(a). The delay was scanned up to 4.8 ps after the arrival of the optical pulse, so the frequency map has a bandwidth of 0.2 THz, approximately one quarter the linewidth of the A_{1g} mode. Figure 2(b) shows the calculation of the Fourier intensity at 2.85 THz, assuming the mode contribution to the intensity is given by Eq. 3 with $\langle u^2_{\boldsymbol{q},i}(t) \rangle$ given by Eq. 2 and with the eigenvectors and frequencies computed from DFPT. Additional extracted coupling constants and the corresponding theoretical predictions for the same point in reciprocal space

Table I. Table of coupling constants $g_{\boldsymbol{q}}$ extracted from various points in the Brillouin zone. Numbers in the first column correspond to the points shown in fig. 2. The third column shows the extracted values, and the fourth column shows theoretical predictions based on DFPT calculations.

Point	$\boldsymbol{q}$ (r.l.u.)	$g_{\boldsymbol{q},\mathrm{exp}}$	$g_{\boldsymbol{q},\mathrm{th}}$
1	(0.11 0.12 0.31)	-1.0	-8.4
2	(-0.27 -0.10 0.18)	-0.7	-6.8
3	(0.22 0.02 -0.39)	-0.8	-6
4	(-0.21 0.35 -0.45)	-1.0	-8.3

are shown in table I. The points on the detector used to extract these coupling constants are shown in fig. 2(a). The extracted and predicted coupling constants are off by approximately one order of magnitude from each other, and roughly correlated in amplitude.

Impulsive optical excitation of hot carriers drives the coherent A_{1g} phonon [17, 21] as well as a continuum of squeezed modes across the Brillouin zone by a second-order Raman-like process [15, 22, 33, 34]. These two effects manifest themselves differently in our data. While the coherent A_{1g} phonon modulates the structure factor for wavevectors near the zone center at Ω, the squeezed modes modulate $\langle u^2_{\boldsymbol{q}} \rangle$ and thus the intensity oscillates at $2\omega_{\boldsymbol{q}}$ across the Brillouin zone, mostly away from $q = 0$ [15, 33, 35, 36]. Hereafter, we refer to this effect as *sudden squeezing*. In addition, the coherent A_{1g} mode resonantly drives the mean-squared displacements of modes at $2\omega_{\boldsymbol{q}} \approx \Omega$, which results in an additional oscillatory component at $2\omega_{\boldsymbol{q}}$, referred hereafter as *resonant squeezing*.

Several features allow us to distinguish the effects of sudden squeezing from resonant squeezing on $\langle u^2_{\boldsymbol{q}}(t) \rangle$. First, the differential change in the mean-square phonon displacements due to the oscillation of the coherent A_{1g} mode should start near zero at $t = 0$ and build up slowly as energy is transferred from the A_{1g} mode into the acoustic mode, as seen in the top trace in Fig. 1 (b). In contrast, sudden squeezing oscillations will peak within a quarter cycle after photoexcitation and decay over time. Second, in a driven parametric oscillator, the drive displacement $A(t)$ is $-\pi/4$ out of phase with the amplitude of the signal and idler displacements $u_{\boldsymbol{q}}$.

We measure the mean-square displacements, $\langle u^2_{\boldsymbol{q}}(t) \rangle$, which results in a $-\pi/2$ phase shift between $\langle u^2_{\boldsymbol{q}}(t) \rangle$ and $A(t)$, as is seen in the phase difference between the traces in Fig. 1 (b), in contrast to directly squeezed phonons, which will be in phase with the coherent A_{1g} mode at moderate squeezing amplitude. Least-squares fitting of the oscillatory parts of the traces shown in Fig. 1 gives a relative phase of $\Delta\phi = 4.5 \pm 0.2$ rad., within the margin of error of $\Delta\phi = -\pi/2$.

Finally, the spectral content of the sudden and resonant squeezed modes are distinct. The parametrically-squeezed modes have the largest oscillations in the mean-square displacements near the resonance $2\omega_{\boldsymbol{q}} = \Omega$. In contrast, sudden squeezing produces a broad continuum of modes with an amplitude that is proportional to $k_B T/\omega^2_{\boldsymbol{q}}$ in the high temperature limit, where T is the (initial) lattice temperature.

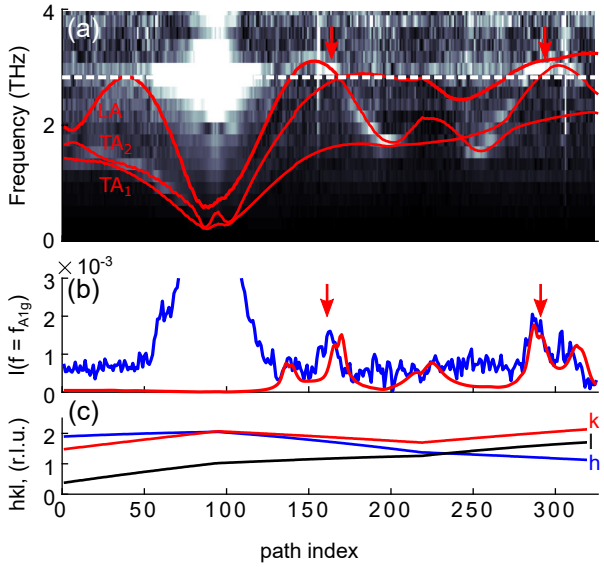

Figure 3. (a) Color online. Lineout along the cut shown in red in Fig. 2(a). The intensity is scaled by ω^2. The bright spot near $q = 0$ at 2.85 THz is from the A_{1g} mode. The second harmonic of the acoustic dispersion is plotted on top of the lineout. The A_{1g} mode frequency is represented by a white dashed line. The squeezing signal is brightest where the phonon branches intersect the A_{1g} frequency (red arrows). (b) Intensity at the 2.85 THz along the lineout shown in (a). Blue is experiment, red is the simulation as described in the text. Arrows point to the same positions along the cut as in (a). (c) The reciprocal lattice positions (h k l) indices (in r.l.u) along the cut.

In Fig. 3 we show the Fourier magnitude along the lineout in reciprocal space given by the red line in Fig. 2 (a). The Fourier transform amplitude is scaled by ω^2 to compensate for the $\propto 1/\omega^2_{\boldsymbol{q}}$ amplitude of the suddenly squeezed modes. The solid red lines in Fig. 3(a) are the second harmonic of the acoustic dispersion relation calculated from DFPT [37] and the dashed white line indicates the frequency of the A_{1g} mode. The calculated frequencies were scaled by approximately 15% to more closely match the measured dispersion. Sudden squeezing is responsible for the intensity of the lower frequencies in Fig. 3(a), mostly from the TA branches. In contrast, the bright features in fig. 3(a) at 2.85 THz and peaks in fig. 3(b) marked with red arrows are due to the parametric resonance. The corresponding momentum transfer, $\boldsymbol{Q} = (h\ k\ l)$ for every point along the lineout is shown in Fig. 3(c), and the resonances occur near $\boldsymbol{Q} = (1.71\ 1.86\ 1.16)$ and $\boldsymbol{Q} = (1.19\ 2.00\ 1.60)$ r.l.u.

In conclusion, we report the first observation of resonant squeezing of acoustic phonons by anharmonic coupling to the A_{1g} mode in bismuth and measure the decay products over a wide range of the Brillouin zone. We have also measured the anharmonic coupling constants for representative decay channels within an order of magnitude of parameters extracted from DFPT calculations. This work demonstrates a method that can measure individual phonon-phonon coupling channels throughout the Brillouin zone. These results should be independent of how the coherent motion at zone center is initiated. Of particular interest is the anharmonicity of zone-center IR-active modes that, when driven strongly by mid-IR laser pulses, have been used to manipulate the macroscopic phase of the material [38]. This approach to measuring phonons away from zone-center can image the short-range lattice fluctuations that couple to macroscopic changes in electronic properties [39]. Furthermore, this generalizes to situations where the driven zone-center boson is not a phonon but some other excitation that couples to collective excitations deep in the Brillouin zone [40].

This work was supported by the U.S. Department of Energy, Office of Science, Office of Basic Energy Sciences through the Division of Materials Sciences and Engineering under Contract No. DE-AC02-76SF00515. C. Uher and T. Bailey acknowledge support from the Department of Energy, Office of Basic Energy Science under Award # DE-SC-0008574. Work at the Tyndall National Institute was supported by Science Foundation Ireland award 12/IA/1601 and the Irish Research Council GOIPG/2015/2784. Measurements were carried out at the Linac Coherent Light Source, a national user facility operated by Stanford University on behalf of the U.S. Department of Energy, Office of Basic Energy Sciences. Preliminary measurements were performed at the Stanford Synchrotron Radiation Lightsource (Beamline 7–2), SLAC National Accelerator Laboratory. We thank Soo Heyong Lee and Wonhyuk Jo for experimental assistance.

* steitelb@slac.stanford.edu

[1] W. Zhong, David Vanderbilt, and K. M. Rabe. First-principles theory of ferroelectric phase transitions for perovskites: The case of BaTiO3. *Physical Review B*, 52(9):6301–6312, 1995.

[2] Charles Kittel. *Introduction to Solid State Physics*. John Wiley & Sons, Inc., New York, 6th edition, 1986.

[3] M. Zebarjadi, K. Esfarjani, M. S. Dresselhaus, Z. F. Ren, and G. Chen. Perspectives on thermoelectrics: from fundamentals to device applications. *Energy Environ. Sci.*, 5(1):5147–5162, 2012.

[4] Alberto Debernardi, Stefano Baroni, and Elisa Molinari. Anharmonic phonon lifetimes in semiconductors from density-functional perturbation theory. *Phys. Rev. Lett.*, 75:1819–1822, Aug 1995.

[5] D. A. Broido, M. Malorny, G. Birner, Natalio Mingo, and D. A. Stewart. Intrinsic lattice thermal conductivity of semiconductors from first principles. *Applied Physics Letters*, 91(23):231922, 2007.

[6] Atsushi Togo, Laurent Chaput, and Isao Tanaka. Distributions of phonon lifetimes in brillouin zones. *Phys. Rev. B*, 91:094306, Mar 2015.

[7] Sergej Krylow, Eeuwe S. Zijlstra, Fairoja Cheenicode Kabeer, Tobias Zier, Bernd Bauerhenne, and Martin E. Garcia. Nonequilibrium dynamics of the phonon gas in ultrafast-excited antimony. *Phys. Rev. Materials*, 1:073601, Dec 2017.

[8] B. N. Brockhouse and A. T. Stewart. Scattering of neutrons by phonons in an aluminum single crystal. *Phys. Rev.*, 100:756–757, Oct 1955.

[9] Stephen William Lovesey. *Theory of thermal neutron scattering: the use of neutrons for the investigation of condensed matter*. Clarendon Press, 1971.

[10] Gordon Leslie Squires. *Introduction to the Theory of Thermal Neutron Scattering*. Courier Corporation, 1978.

[11] Michael Krisch and Francesco Sette. *Inelastic X-Ray Scattering from Phonons*, pages 317–370. Springer Berlin Heidelberg, Berlin, Heidelberg, 2007.

[12] Eberhard Burkel. Phonon spectroscopy by inelastic x-ray scattering. *Reports on Progress in Physics*, 63(2):171, 2000.

[13] Alfred Q. R. Baron. *High-Resolution Inelastic X-Ray Scattering I: Context, Spectrometers, Samples, and Superconductors*, pages 1–68. Springer International Publishing, Cham, 2014.

[14] Alfred Q. R. Baron. *High-Resolution Inelastic X-Ray Scattering II: Scattering Theory, Harmonic Phonons, and Calculations*, pages 1–32. Springer International Publishing, Cham, 2014.

[15] M. Trigo, M. Fuchs, J. Chen, M. P. Jiang, M. Cammarata, S. Fahy, D. M. Fritz, K. Gaffney, S. Ghimire, A. Higginbotham, S. L. Johnson, M. E. Kozina, J. Larsson, H. Lemke, A. M. Lindenberg, G. Ndabashimiye, F. Quirin, K. Sokolowski-Tinten, C. Uher, G. Wang, J. S. Wark, D. Zhu, and D. A. Reis. Fourier-transform inelastic x-ray scattering from time-and momentum-dependent phonon-phonon correlations. *Nature Physics*, 9(12):790–794, oct 2013.

[16] Stephen Fahy, Éamonn D. Murray, and David A. Reis. Resonant squeezing and the anharmonic decay of coherent phonons. *Phys. Rev. B*, 93:134308, Apr 2016.

[17] T. K. Cheng, S. D. Brorson, a. S. Kazeroonian, J. S. Moodera, G. Dresselhaus, M. S. Dresselhaus, and E. P. Ippen. Impulsive excitation of coherent phonons observed in reflection in bismuth and antimony. *Applied Physics Letters*, 57(10):1004, 1990.

[18] T. Garl, E. G. Gamaly, D. Boschetto, A. V. Rode, B. Luther-Davies, and A. Rousse. Birth and decay of coherent optical phonons in femtosecond-laser-excited bismuth. *Phys. Rev. B*, 78:134302, Oct 2008.

[19] Muneaki Hase, Kunie Ishioka, Masahiro Kitajima, Kiminori Ushida, and Shunichi Hishita. Dephasing of coherent phonons by lattice defects in bismuth films. *Applied Physics Letters*, 76(10):1258–1260, 2000.

[20] Klaus Sokolowski-Tinten, Christian Blome, Juris Blums, Andrea Cavalleri, Clemens Dietrich, Alexander Tarasevitch, Ingo Uschmann, Eckhard Förster, Martin Kammler, Michael Horn-von Hoegen, and Dietrich von der Linde. Femtosecond X-ray measurement of coherent lattice vibrations near the Lindemann stability limit. *Na-*

ture, 422(6929):287–289, mar 2003.

[21] D M Fritz, D A Reis, B Adams, and R A Akre. Ultrafast bond softening in bismuth: Mapping a solid's interatomic potential with X-rays. *Science*, 315(February):633–637, 2007.

[22] S. L. Johnson, P. Beaud, E. Vorobeva, C. J. Milne, É. D. Murray, S. Fahy, and G. Ingold. Directly Observing Squeezed Phonon States with Femtosecond X-Ray Diffraction. *Physical Review Letters*, 102(17):175503, apr 2009.

[23] Xin Ma and William Rhodes. Squeezing in harmonic oscillators with time-dependent frequencies. *Phys. Rev. A*, 39:1941–1947, Feb 1989.

[24] Xuedong Hu and Franco Nori. Squeezed Phonon States: Modulating Quantum Fluctuations of Atomic Displacements. *Physical Review Letters*, 76(13):2294–2297, 1996.

[25] More generally, non-degenerate coupling to different branches (i and j) is also possible, though we do not observe this process in this experiment. In this case the parametric resonance condition is $\Omega = \omega_{\boldsymbol{q}i} \pm \omega_{\boldsymbol{q}j}$.

[26] Matthieu Chollet, Roberto Alonso-Mori, Marco Cammarata, Daniel Damiani, Jim Defever, James T. Delor, Yiping Feng, James M. Glownia, J. Brian Langton, Silke Nelson, Kelley Ramsey, Aymeric Robert, Marcin Sikorski, Sanghoon Song, Daniel Stefanescu, Venkat Srinivasan, Diling Zhu, Henrik T. Lemke, and David M. Fritz. The X-ray Pump-Probe instrument at the Linac Coherent Light Source. *Journal of Synchrotron Radiation*, 22(November 2014):503–507, 2015.

[27] Sven Herrmann, Sébastien Boutet, Brian Duda, David Fritz, Gunther Haller, Philip Hart, Ryan Herbst, Christopher Kenney, Henrik Lemke, Marc Messerschmidt, Jack Pines, Aymeric Robert, Marcin Sikorski, and Garth Williams. CSPAD-140k : A versatile detector for LCLS experiments. *Nuclear Instruments and Methods in Physics Research*, 718:550–553, 2013.

[28] B. Arnaud and Y. Giret. Electron Cooling and Debye-Waller Effect in Photoexcited Bismuth. *Physical Review Letters*, 110(1):016405, jan 2013.

[29] Lutz Waldecker, Thomas Vasileiadis, Roman Bertoni, Ralph Ernstorfer, Tobias Zier, Felipe H. Valencia, Martin E. Garcia, and Eeuwe S. Zijlstra. Coherent and incoherent structural dynamics in laser-excited antimony. *Phys. Rev. B*, 95:054302, Feb 2017.

[30] J. Faure, J. Mauchain, E. Papalazarou, M. Marsi, D. Boschetto, I. Timrov, N. Vast, Y. Ohtsubo, B. Arnaud, and L. Perfetti. Direct observation of electron thermalization and electron-phonon coupling in photoexcited bismuth. *Phys. Rev. B*, 88:075120, Aug 2013.

[31] We note that a lower bound for g_q can be obtained without prior knowledge of the mode frequencies, eigenvectors and decay rates. The values obtained in this manner differ by less than a factor of two from our reported results.

[32] J. J. Li, J. Chen, D. A. Reis, S. Fahy, and R. Merlin. Optical probing of ultrafast electronic decay in bi and sb with slow phonons. *Phys. Rev. Lett.*, 110:047401, Jan 2013.

[33] T. Henighan, M. Trigo, M. Chollet, J. N. Clark, S. Fahy, J. M. Glownia, M. P. Jiang, M. Kozina, H. Liu, S. Song, D. Zhu, and D. a. Reis. Control of two-phonon correlations and the mechanism of high-wavevector phonon generation by ultrafast light pulses. *Physical Review B*, 94(2):020302, jul 2016.

[34] G. A. Garrett, A. G. Rojo, A. K. Sood, J. F. Whitaker, and R. Merlin. Vacuum squeezing of solids: Macroscopic quantum states driven by light pulses. *Science*, 275(5306):1638–1640, 1997.

[35] Diling Zhu, Aymeric Robert, Tom Henighan, Henrik T. Lemke, Matthieu Chollet, J. Mike Glownia, David a. Reis, and Mariano Trigo. Phonon spectroscopy with sub-meV resolution by femtosecond x-ray diffuse scattering. *Physical Review B*, 92(5):054303, aug 2015.

[36] Eeuwe S. Zijlstra, Alan Kalitsov, Tobias Zier, and Martin E. Garcia. Squeezed thermal phonons precurse nonthermal melting of silicon as a function of fluence. *Phys. Rev. X*, 3:011005, Jan 2013.

[37] É Murray, S Fahy, D Prendergast, T Ogitsu, D Fritz, and D Reis. Phonon dispersion relations and softening in photoexcited bismuth from first principles. *Physical Review B*, 75(18):184301, may 2007.

[38] M Först, C Manzoni, S Kaiser, Y Tomioka, Y Tokura, R Merlin, and A Cavalleri. Nonlinear phononics as an ultrafast route to lattice control. *Nature Physics*, 7:854–856, 2011.

[39] M. Mitrano, A. Cantaluppi, D. Nicoletti, S. Kaiser, A. Perucchi, S. Lupi, P. Di Pietro, D. Pontiroli, M. Riccò, S. R. Clark, D. Jaksch, and A. Cavalleri. Possible light-induced superconductivity in k3c60 at high temperature. *Nature*, 530(7591):461–464, Feb 2016. Letter.

[40] H. Y. Liu, I. Gierz, J. C. Petersen, S. Kaiser, A. Simoncig, A. L. Cavalieri, C. Cacho, I. C. E. Turcu, E. Springate, F. Frassetto, L. Poletto, S. S. Dhesi, Z.-A. Xu, T. Cuk, R. Merlin, and A. Cavalleri. Possible observation of parametrically amplified coherent phasons in $k_{0.3}moo_3$ using time-resolved extreme-ultraviolet angle-resolved photoemission spectroscopy. *Phys. Rev. B*, 88:045104, Jul 2013.